Electronic Supplementary Material (ESI) for Physical Chemistry Chemical Physics.

Supplementary Information

Significantly enhanced phonon mean free path and thermal conductivity by percolation of silver nanoflowers

Daewoo Suh,[a] Sanghoon Lee,[b] Chenchen Xu,[b] Agha Aamir Jan[a] and Seunghyun Baik*[a]

[a]*School of Mechanical Engineering, Sungkyunkwan University, Suwon 16419, Korea*

[b]*Department of Energy Science, Sungkyunkwan University, Suwon 16419, Korea*

**E-mail: sbaik@me.skku.ac.kr*

Table S1. Thermal conductivity of commercially available soft isotropic TIMs.

Company	Product code	Filler	Polymer matrix	Total filler fraction	Thermal conductivity [W m^{-1} K^{-1}]
3M	5519	Ceramic	Silicone elastomer	N/A	5.0
Laird	Tflex SF800	Ceramic	Silicone-free elastomer	N/A	7.8
	Tpcm 780	Al + Zinc oxide	Silicone-free elastomer	Al powder (60–80 wt%) Zinc oxide (1–16 wt%)	5.4
ShinEtsu	TC-TAG-8	N/A	Silicone elastomer	N/A	8.0
	X-23-7921-5	Al + Zinc oxide	Silicone elastomer	Aluminum (> 70 %) Zinc Oxide (< 25 %)	6.0
T-global technology	TG4040	Aluminum oxide	Silicone elastomer	Aluminum oxide (20%)	4.0
	TG6050	Aluminum oxide	Silicone elastomer	Aluminum oxide (20%)	6.0
	TGX-2	Aluminum oxide	Silicone elastomer	Aluminum oxide (35%)	12.0

Table S2. Thermal conductivity comparison of Ag NF-PU (Ag = 38 vol%) film with soft TIMs in literature.

Filler type	Filler anisotropy	Filler	Polymer matrix	Total filler fraction [vol% or wt%]	Thermal conductivity [W m^{-1} K^{-1}] Aligned-direction, Perpendicular	Ref.
Ceramic	Anisotropic	Boron nitride	Poly(vinyl alcohol)	27 vol%	8.4 (Aligned) 1.6 (Perpendicular)	S1
		Boron nitride	Polyolefin elastomer	43.8 vol%	6.9 (Aligned) 0.7 (Perpendicular)	S2
		Boron nitride	Polyurethane	30 wt%	5.2 (Aligned) 1.3 (Perpendicular)	S3
		Boron nitride	Nanofibrillated cellulose	50 wt%	145.7 (Aligned) N/A (Perpendicular)	S4
		Boron nitride	Epoxy	50 vol%	30 (Aligned)	S5
		Boron nitride	Polyurethane	50 wt%	10.3 (Aligned)	S6
	Isotropic	Aluminum nitride	Silicone elastomer	28.6 wt%	1.3	S7
Carbon	Anisotropic	Natural graphite	Polyolefin elastomer	49.3 vol%	13.3 (Aligned) 0.8 (Perpendicular)	S8
		Graphite nanosheet	Epoxy	33 vol%	80 (Aligned) 10.7 (Perpendicular)	S9
		Vertically aligned carbon fiber	Fluorinated rubber	13.2 wt%	23.3 (Aligned) 0.4 (Perpendicular)	S10
Metal	Isotropic	Gallium-based liquid metal alloy	Polydimethyl siloxane	66.1 vol%	2.2	S11
		EGaIn liquid metal alloy	Silicone elastomer	50 vol%	4.7	S12
		Copper nanowire	Polyurethane	4.2 vol%	0.6	S13
		Gold nanowire	Polydimethyl siloxane	3 vol%	5	S14
Metal	Isotropic	Silver nanoflower	Polyurethane	38 vol% (84.9 wt%)	42.4	This study

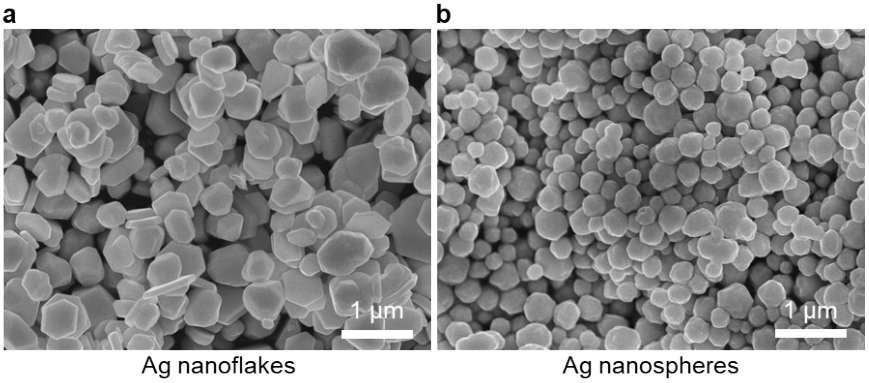

Figure S1. SEM images of Ag nanoflakes (a) and Ag nanospheres (b). The average sizes of Ag nanoflakes and Ag nanospheres were ~500 and ~300 nm.

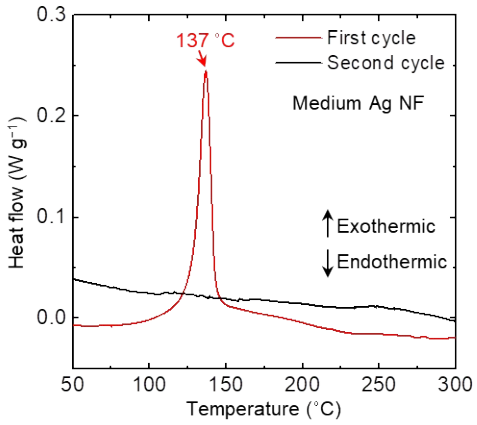

Figure S2. Differential scanning calorimetry analysis was carried out two consecutive times using the same medium Ag NFs.

Table S3. The weight and volume concentration of Ag fillers in the Ag-PU films.

Mass of Ag fillers [g]	Mass of polymer [g]	Weight percentage of Ag fillers [wt%]	Volume percentage of Ag fillers [vol%]
0.6060	0.3	66.9	18
0.7786		72.2	22
0.9699		76.4	26
1.1831		79.8	30
1.4221		82.6	34
1.5528		83.8	36
1.6919		84.9	38

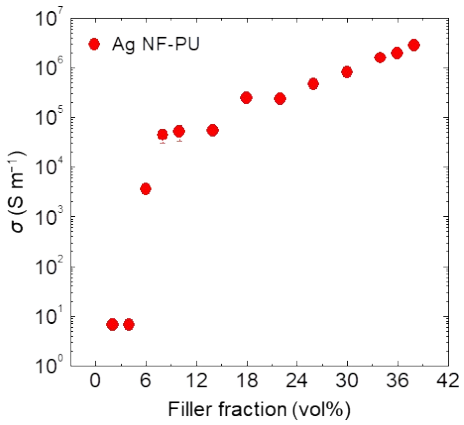

Figure S3. The electrical conductivity of Ag NF-PU films as a function of the Ag NF concentration.

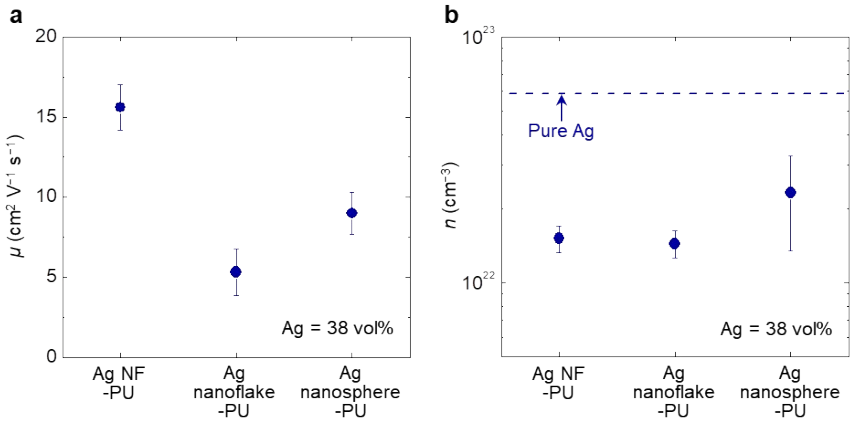

Figure S4. The carrier mobility (a) and concentration (b) of Ag-PU (Ag = 38 vol%) films. The carrier concentration of pure Ag is designated by the dashed line.

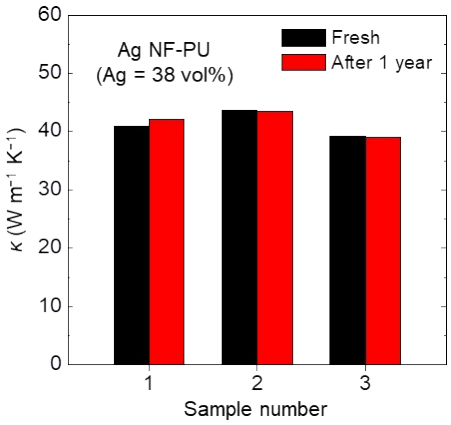

Figure S5. The long-term air stability of Ag NF-PU (Ag = 38 vol%) films. The thermal conductivity of 3 specimens was invariant for 1 year.

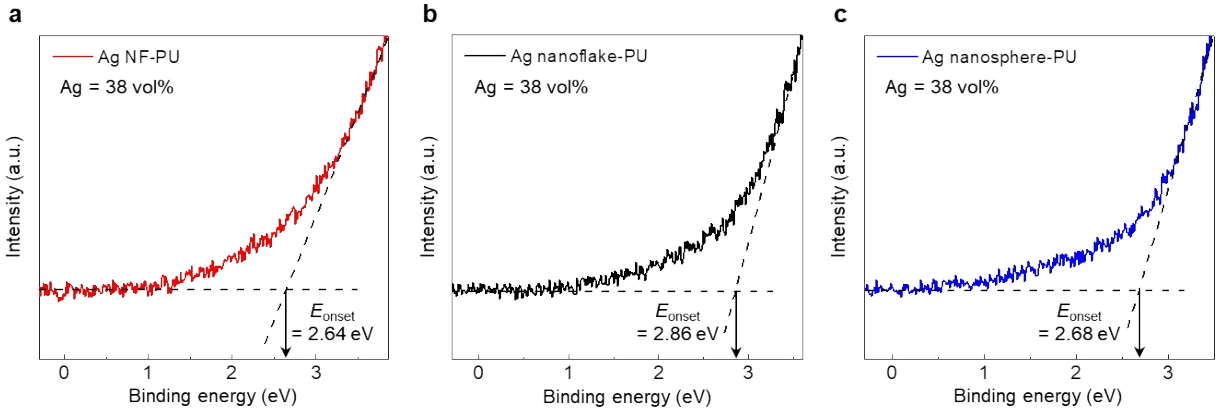

Figure S6. The onset region of UPS spectra was magnified, and E_{onset} was obtained by tangent analysis. (a) Ag NF-PU (Ag = 38 vol%) film. (b) Ag nanoflake-PU (Ag = 38 vol%) film. (c) Ag nanosphere-PU (Ag = 38 vol%) film.

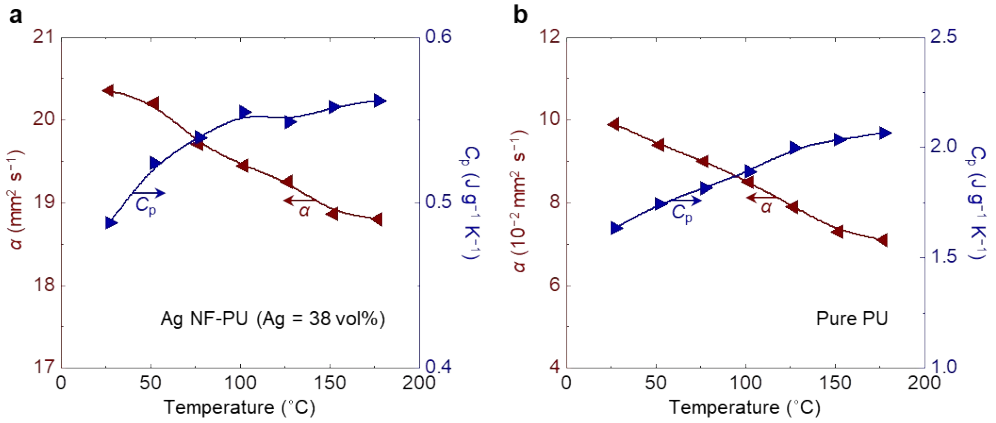

Figure S7. The temperature-dependent thermal diffusivity and mass specific heat capacity of Ag NF-PU (Ag = 38 vol%) film (a) and pure PU film (b).

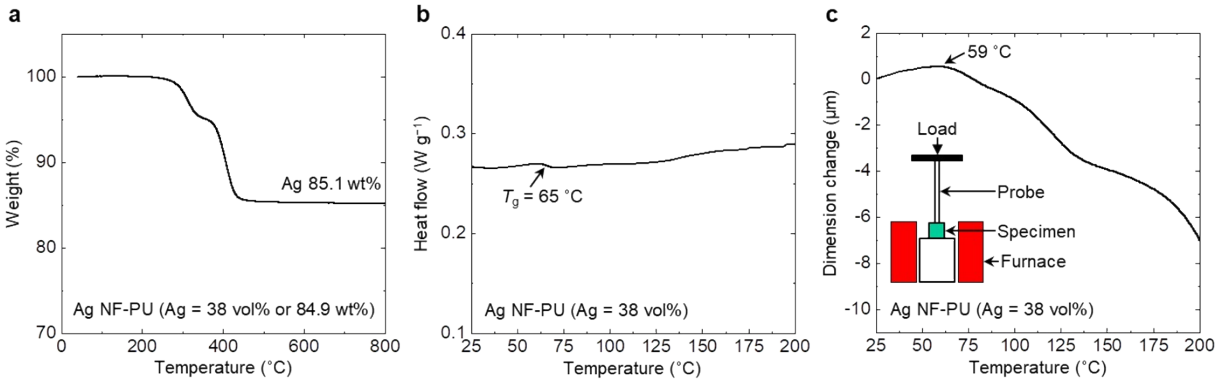

Figure S8. The thermal stability and thermal expansion of Ag NF-PU (Ag = 38 vol%) film. (a) Thermogravimetric analysis. The residual Ag concentration (85.1 wt%) in the Ag NF-PU film was close to the nominal concentration (84.9 wt%). (b) Differential scanning calorimetry analysis. (c) Thermomechanical analysis to evaluate thermal expansion of the specimen. A schematic of the measurement setup is provided in the inset.

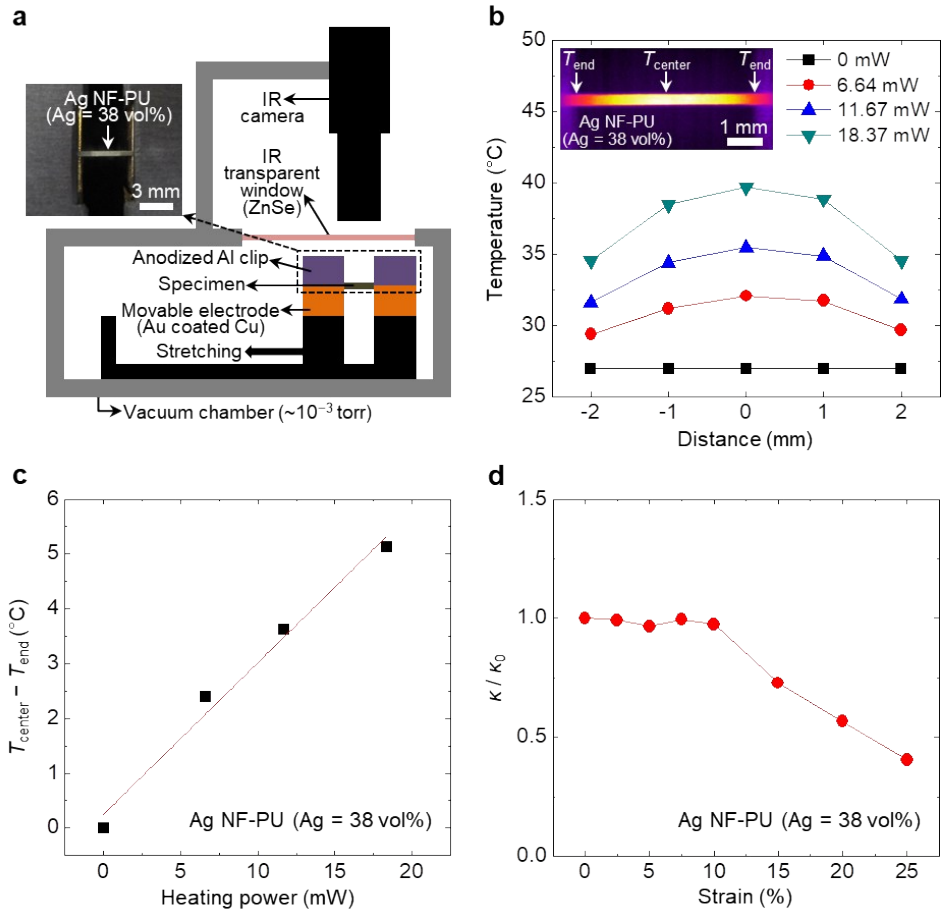

Figure S9. The thermal conductivity measurement of Ag NF-PU (Ag = 38 vol%) film as a function of strain. (a) Schematic of the measurement setup. The Ag NF-PU (Ag = 38 vol%) film was cut into 1-dimensional strip and Joule-heated. An optical image of the film is provided in the inset. The film was stretched by a movable gold-coated copper electrode (heat sink), and temperature distribution was measured by an infrared camera. (b) Temperature profiles of the Joule-heated film at different heating powers (strain = 0%). A false-colored infrared image is provided in the inset. (c) The slope between the temperature difference ($T_{center} - T_{end}$) and heating power was used to calculate the thermal conductivity (strain = 0%). (d) The variation in thermal conductivity of Ag NF-PU (Ag = 38 vol%) film is shown as a function of strain.

The thermal conductivity (κ) of Ag NF-PU (Ag = 38 vol%) film was investigated as a function of strain using a recently-built setup.[S15] A detailed discussion about the measurement setup and theory were provided elsewhere,[S15] and a brief description is provided below. The Ag NF-PU (Ag = 38 vol%) film was cut into 1-dimensional strip ($20\times0.5\times0.1$ mm^3) and clamped between movable gold-coated copper electrodes (Figure S9a). The electrode movement was controlled using a stepping motor. The film was Joule-heated by a direct current power supply (Keithley, 2280S-32-6), and the electrodes

worked as a heat sink. The temperature distribution was measured by an infrared camera (FLIR, A325sc) through a ZnSe viewport. The experiment was carried out in a vacuum chamber (Ecopia, ~10^{-3} torr) to neglect convection heat loss.[S15]

Figure S9b shows temperature profiles of the Joule-heated Ag NF-PU (Ag = 38 vol%) film at different heating powers. A steady-state symmetric temperature profile was obtained because the electrodes at both ends worked as a heat sink. The temperature increased as the heating power increased.

The κ was calculated using the 1-dimensional Fourier's conduction model in a steady state, and the detailed derivation is provided elsewhere.[S15,S16]

$$T_x = T_{end} + \frac{q}{2\kappa}(L^2 - x^2) \quad \text{(S1)}$$

The volumetric Joule heat generation is given by $q = UI/2A_cL$, where U is the voltage drop across the film, and I is the supplied current. A_c and L are the cross-sectional area and half length of the film. The thickness and A_c of the film were measured outside the chamber under the identical strain condition. T_{end} is the temperature at the end ($x = L$). The κ was finally obtained from the slope between the electrical power (UI) and ($T_{center} - T_{end}$), where T_{center} is the temperature at the center ($x = 0$), as shown in Figure S9c.[S15,S16]

$$\kappa = \frac{L}{4A_c} \cdot \frac{UI}{(T_{center} - T_{end})} \quad \text{(S2)}$$

As shown in Figure S9d, the normalized thermal conductivity of Ag NF-PU (Ag = 38 vol%) film was well-maintained up to 10% strain and then monotonically decreased to 41% as the film was further stretched to 25% strain. This could be due to increased axial distance between Ag NFs with further stretching.

References

[S1] J. Zhang, X. Wang, C. Yu, Q. Li, Z. Li, C. Li, H. Lu, Q. Zhang, J. Zhao, M. Hu and Y. Yao, *Compos. Sci. Technol.* 2017, **149**, 41.

[S2] C. Feng, L. Bai, R. Bao, Z. Liu, M. Yang, J. Chen and W. Yang, *Adv. Compos. Hybrid Mater.* 2018, **1**, 160.

[S3] F. Yuan, W. Jiao, F. Yang, W. Liu, Z. Xua and R. Wang, *RSC Adv.* 2017, **7**, 43380.

[S4] H. Zhu, Y. Li, Z. Fang, J. Xu, F. Cao, J. Wan, C. Preston, B. Yang and L. Hu, *ACS Nano* 2014, **8**, 3606.

[S5] W. Song, P. Wang, L. Cao, A. Anderson, M. J. Meziani, A. J. Farr and Y. Sun, *Angew. Chem. Int. Ed.* 2012, **51**, 6498.

[S6] H. Hong, S. M. Kwan, D. S. Lee, S. M. Kim, Y. H. Kim, J. S. Lim, J. Y. Hwang and H. S. Jeong, *Compos. Sci. Technol.* 2017, **152**, 94.

[S7] L. Tian, Y. Wang, E. Jin, Y. Li, R. Wang and Y. Shang, *Adv. Mech. Eng.* 2017, **9**, 1.

[S8] C. Feng, L. Bai, Y. Shao, R. Bao, Z. Liu, M. Yang, J. Chen, H. Ni and W. Yang, *Adv. Mater. Interfaces* 2018, **5**, 1700946.

[S9] L. M. Veca, M. J. Meziani, W. Wang, X. Wang, F. Lu, P. Zhang, Y. Lin, R. Fee, J. W. Connell and Y. Sun, *Adv. Mater.* 2009, **21**, 2088.

[S10] K. Uetani, S. Ata, S. Tomonoh, T. Yamada, M. Yumura and K. Hata, *Adv. Mater.* 2014, **26**, 5857.

[S11] S. H. Jeong, S. Chen, J. Huo, E. K. Gamstedt, J. Liu, S. Zhang, Z. Zhang, K. Hjort and Z. Wu, *Sci. Rep.* 2015, **5**, 18257.

[S12] M. D. Bartlett, N. Kazem, M. J. Powell-Palma, X. Huang, W. Sun, J. A. Malen and C. Majidi, *Proc. Natl. Acad. Sci. U. S. A.* 2017, **114**, 2143.

[S13] A. Rai and A. L. Moore, *Compos. Sci. Technol.* 2017, **144**, 70.

[S14] N. Balachander, I. Seshadri, R. J. Mehta, L. S. Schadler, T. Borca-Tasciuc, P. Keblinski and G. Ramanath, *Appl. Phys. Lett.* 2013, **102**, 093117.

[S15] A. A. Jan, D. Suh, S. Bae and S. Baik, *Nanoscale* 2018, **10**, 17799.

[S16] G. Xin, T. Yao, H. Sun, S. M. Scott, D. Shao, G. Wang and J. Lian, *Science* 2015, **349**, 1083.